Tectonophysics 761 (2019) 1–15

Contents lists available at ScienceDirect

Tectonophysics

journal homepage: www.elsevier.com/locate/tecto

Crustal melting beneath orogenic plateaus: Insights from 3-D thermo-mechanical modeling

Lin Chen[a,*], Xiaodong Song[b], Taras V. Gerya[c], Tao Xu[a,d], Yun Chen[a]

[a] State Key Laboratory of Lithospheric Evolution, Institute of Geology and Geophysics, Chinese Academy of Sciences, Beijing 100029, China
[b] Department of Geology, University of Illinois at Urbana-Champaign, IL 61801, USA
[c] Institute of Geophysics, ETH-Zurich, CH-8092 Zurich, Switzerland
[d] CAS Center for Excellence in Tibetan Plateau Earth Sciences, Beijing 100101, China

ARTICLE INFO

Keywords:
Numerical modeling
Continental collision
Crustal melting
Radioactive heating
Shear heating
Tibetan plateau

ABSTRACT

Mid-crustal melting is widely documented under orogenic plateaus. However, the mechanism for its generation and its role in the evolution of orogenic plateaus remain poorly understood. Here we investigate the physical controls and consequences of crustal melting in plateau evolution using 3-D thermo-mechanical modeling method. Our simulations demonstrate that the convergence causes orogenic crust to have more upper crustal compositions and more radiogenic elements. The persistent radioactive and shear heating provides heat source required for in situ partial melting of felsic rocks at mid-crustal depths. Slower convergence rate favors earlier emergence and larger concentration of mid-crustal melt. Radioactive heating accumulated during crustal thickening plays the primary role in generating mid-crustal partial melting, which is consistent with previous 2-D model results. Shear heating promotes crustal melting, but its role is secondary to radioactive heating. Our simulations also show that basal heating produces a broad-area increase of the crust temperature and surface elevation and, to a lesser extent, promotes mid-crustal melting, because convergence-driven heat advection dominates the transport of the newly-added heat. The significant mid-crustal melting dramatically reduces the viscosity of the middle crust and eventually leads to channelized outward flow of the melt-weakened layer. This has the potential to cause mechanical decoupling of the layers above and below the melt channel and the marginal dominance of mid-crustal melting. We suggest that the widespread low velocity or resistivity zones observed in Tibet are caused by interconnected mid-crustal melting, which is an inherent feature of large hot orogenic plateaus.

1. Introduction

The formation of a continental plateau follows crustal thickening driven by plate convergence. As the continental crust thickens, it can become sufficiently hot to initiate melting (Brown, 2010; Jamieson et al., 2011; Vanderhaeghe and Teyssier, 2001). There is ample evidence for crustal melting beneath continental plateaus and orogens. For example, geophysical observations, including low seismic velocity zone (e.g., Bao et al., 2015; Yang et al., 2012), high Poisson's ration (e.g., Owens and Zandt, 1997), high seismic wave attenuation (e.g., Zhao et al., 2013), mid-crustal “bright spots” (e.g., Nelson et al., 1996), and high conductance features (e.g., Bai et al., 2010; Unsworth et al., 2005; Wei et al., 2001) found within the crust of the Tibetan plateau, implicates the presence of crustal partial melt or aqueous fluid accumulation. The exhumed muscovite-bearing leucogranites and migmatites intruded in the Greater Himalayan Sequence along the Himalayan orogen (e.g., Cottle et al., 2015; Harris, 2007) reflect that the orogenic crust is affected by deep crustal melting. Geochemical and petrological studies at specific rift or fault zones, provide more convincing evidence for the occurrence of a partially molten zone in the mid- to lower crust in central and northern Tibet (Ding et al., 2003; Wang et al., 2010), and constrain the existence of the deep crustal melting from middle Eocene to Quaternary times (Wang et al., 2012). Although both geophysical and petrological-geochemical data point to deep crustal melting beneath the Tibetan plateau, there is much controversy over whether deep crustal melting is pervasive throughout the plateau or restricted to the rifts or faults (DeCelles et al., 2002; Hacker et al., 2000; Hetenyi et al., 2011).

Laboratory experiments demonstrate that crustal melting can lead to a dramatic reduction in its strength (Rosenberg and Handy, 2005; Rosenberg et al., 2007). Previous 2-D thermo-mechanical models linked the presence of melt-weakened crust to ductile flow and exhumation of

* Corresponding author at: No. 19 Beitucheng West Road, Beijing 100029, China.
E-mail address: chenlin@mail.iggcas.ac.cn (L. Chen).

https://doi.org/10.1016/j.tecto.2019.03.014
Received 20 July 2018; Received in revised form 21 March 2019; Accepted 25 March 2019
Available online 15 April 2019
0040-1951/

deeply buried continental crust (Beaumont et al., 2001, 2004; Whitney et al., 2009; Rey et al., 2010). The low-viscosity nature of a partial melting layer has the potential to decouple the motion between the overlying crust and underlying lithospheric mantle. As a result, the crustal channel flow hypothesis has been proposed, on the basis of observations and numerical models, to understand the evolution of the Tibetan plateau (Grujic et al., 1996, 2002; Royden et al., 1997; Clark and Royden, 2000; Shen et al., 2001; Cook and Royden, 2008). However, whether the presence of crustal melting really leads to deformation coupling and crustal channel flow is still poorly understood. The role of the crustal channel flow in plateau evolution has been studied by several groups using numerical models (e.g., Royden et al., 1997; Beaumont et al., 2001, 2004; Rey et al., 2010), yet these models are either two-dimensional or purely mechanical. The crustal deformation during continental collision is a three-dimensional process involving both thermal and mechanical behaviors. For example, orogen-perpendicular thrust faulting along the frontal thrust system is accompanied by hinterland orogen-parallel extensional and strike-slip faulting at the Himalayan-Tibetan orogenic system (e.g., Styron et al., 2011). Seismic ambient noise data also reveal that the mid-crustal low velocity zones are predominant near the periphery of Tibet (Yang et al., 2012). These 3-D features in collision orogens cannot be replicated by 2-D (e.g., Beaumont et al., 2001, 2004) or purely-mechanical models (e.g., England and Houseman, 1988; Cook and Royden, 2008).

Recently, 3-D thermo-mechanical models have been used to investigate the influence of preexisting lateral lithospheric strength heterogeneities on the styles of orogenic plateau growth (Chen and Gerya, 2016). They predicted orogen-parallel spreading of an orogenic plateau and found a mid-crustal partial melting layer self-consistently emerges at the later stage of the plateau evolution. The presence of this layer was speculatively attributed to enhanced radioactive and shear heating during crustal thickening. However, the physical controls for the occurrence of mid-crustal partial melting and its role in orogenic plateau evolution were not explored in that study.

To better understand the dynamics of deep crustal melting and its role in the growth of orogenic plateaus, we have extended the numerical model presented in Chen and Gerya (2016) by including the initial steady-state temperature field and more realistic melt-weakening effect of rock melting (Katz et al., 2006). Furthermore, we examine the influences of radioactive, shear and basal heating on crustal melting using systematical 3-D thermo-mechanical simulations. Our focus is on the physical controls for the generation of deep crustal melting and its consequences in orogenic plateau evolution, including topographic expression and crustal deformation behavior. The model results are applied to reconciling the regional geophysical observations with the scattered petrological-geochemical data beneath the Tibetan plateau. Our study was mainly inspired by the findings of a dominance of low seismic velocity or high conductance zones at the Tibetan middle crust (e.g., Yang et al., 2012; Bao et al., 2015; Unsworth et al., 2005; Bai et al., 2010), but the implications may be applicable to other orogens or plateaus.

2. Model setup

The numerical simulations are conducted in three dimensions using the thermo-mechanical code I3ELVIS (Gerya, 2010). The code combines a conservative finite difference method with a non-diffusive marker-in-cell technique to solve the energy, momentum, and mass conservation equations. The energy conservation equation includes radiogenic, adiabatic and shear heat sources (Chen and Gerya, 2016). Shear heating (H_s) is associated with dissipation of the mechanical energy during plastic deformation and can be calculated via the deviatoric stresses (σ_{ij}') and strain rates ($\dot{\varepsilon}_{ij}$) as follows (Gerya, 2010): $H_s = \sigma'_{ij}\dot{\varepsilon}_{ij}$. The inclusion of various heat sources allows us to evaluate the effects of different heat productions on crustal melting. Another heat source that may contribute to crustal melting is basal heating arising from slab breakoff or lithosphere delamination (e.g., Bird, 1979; Jimenez-Munt and Platt, 2006). For the purpose of simplification, here basal heating is implemented by removing the lithosphere mantle, i.e., making the crust contact directly with the asthenosphere. A sticky air layer is placed at the top of the model to capture the evolution of topography (e.g., Crameri et al., 2012). The rheological model combines Mohr-Coulomb and diffusion-dislocation creep (e.g., Chen and Gerya, 2016). A linear melting model is employed to define the degree of melting (f) for crustal rocks (Burg and Gerya, 2005). When the melt fraction exceeds 0.5% (f_0), the melt-weakening effect on viscosity (η) starts to work such that the effective viscosity (η_{eff}) (Katz et al., 2006): $\eta_{eff} = \eta \exp(-28 * (f - f_0))$.

The model setup is similar to that used in the previous study of Chen and Gerya (2016). The computational domain is 1000 × 200 × 1000 km (in the order of x, y and z). It is resolved by 501 × 101 × 501 grid points with a uniform resolution of 2 × 2 × 2 km (Fig. 1). There are over 200million Lagrangian markers randomly distributed in the model domain, which are used to assign physical properties, including viscosity, plastic strain, temperature etc. Such a 3-D high-resolution scheme enables us to fully capture the crustal processes in a large horizontal size (1000 × 1000 km) comparable to the nature, but this limits the vertical model size (200 km) owing to the computational difficulty. The mechanical boundary conditions are free slip at the back wall (z = 1000 km) and at both the left and right boundaries (x = 0 and 1000 km). The lower boundary is permeable, where an infinity-like external free slip condition is imposed (e.g., Burg and Gerya, 2005). It is implemented by observing the following rules at the lower boundary: $\partial v_x/\partial y = 0$, $\partial v_z/\partial y = 0$, and $\partial v_y/\partial y = -v_y/\Delta y_{external}$, where v_i is the component of the velocity vector and $\Delta y_{external}$ is the vertical distance from the lower boundary to the external boundary. It implies that free slip is satisfied at $\Delta y_{external}$ below the base of the model domain. A constant velocity is imposed at the first half of the front wall (i.e., x = 0–500 km) to simulate convergence through this region, while the free slip boundary condition is used for the second half of the front wall (i.e., x = 500–1000 km). The constant velocity boundary corresponds to a time-dependent boundary force exerting at the first half of the front wall (Fig. S1). This boundary condition is a simplification to the India-Asia collision, which only considers the northward push derived from the Indian continent subduction and does not account for the subduction process itself. It is noteworthy that changing the boundary condition for the right and back walls from free slip to no slip does not alter significantly the model results (Fig. S2).

The initial temperature field is calculated by solving the steady-state heat conduction equation at the lithospheric scale with a given surface heat flow and a surface temperature of 0°C, where thermal conductivity is rock type- and temperature-dependent (see Table 1). The lithosphere-asthenosphere boundary is defined to be at the 1350°C isotherm. A geothermal gradient of 0.5°C/km is initially prescribed for the asthenosphere. The upper thermal boundary keeps a constant value of 0°C, and all the vertical thermal boundaries keep zero heat flux. Similarly, an infinity-like external constant temperature condition is imposed at the lower thermal boundary (e.g., Burg and Gerya, 2005). It is implemented by following the rule of $\partial T/\partial y = (T_e - T)/\Delta y_t$, where T_e is the temperature at the external boundary and Δy_t (200 km) is the vertical distance from the lower thermal boundary to the external thermal boundary, implying that the constant temperature condition is satisfied at 200 km below the model base. This condition allows the temperature and heat flux at the model base to adjust spontaneously during simulation.

The model domain is initially composed of two continental lithospheres with different characters (Fig. 1a). A relatively hot continental lithosphere is emplaced at the corner situated in the region of 0 ≤ x ≤ 500 and 0 ≤ z ≤ 500, simulating an embryonic orogenic plateau (proto-plateau, also known as pro-lithosphere) present at the very beginning of the continental collision. This assumption is supported by

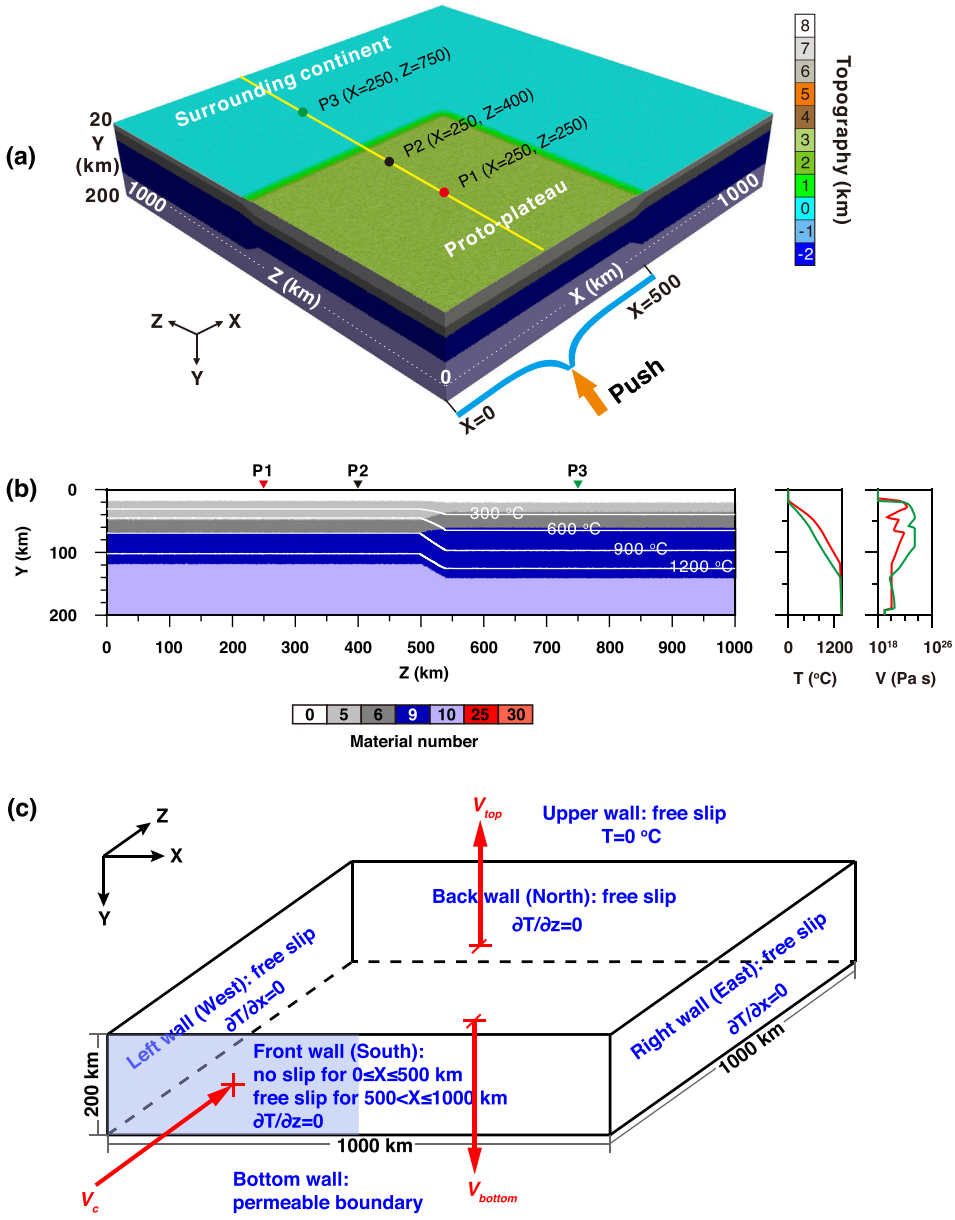

Fig. 1. Model setup. (a) The 3-D model domain (1000 × 200 × 1000 km). The colors covering the top of the model indicate the magnitude of topography as shown in the vertical color bar, while the colors covering the side walls indicate different rock types as in the color bar in (b). The light green-colored area represents the proto-orogenic plateau, and the cyan-colored area represents the surrounding continent. The blue parenthesis shows the scope in which convergence is imposed, and the orange arrow shows the direction of convergence. (b) Cross-section of material field through the plane of x = 250, as shown by the yellow line in (a). White lines are isotherms measured in Celsius. Material numbers represent different rock types, with: 0-sticky air; 5-upper continental crust; 6-lower continental crust; 9-lithospheric mantle; 10-asthenosphere; 25-partially molten continental crust; 30-partially molten asthenosphere (peridotite). The partially molten rocks do not appear in (a), but appears in some figures below. The inverted triangles in (b) indicate localities, at which the topography, viscosity or temperature are shown below. The temperature (T) and viscosity (V) for two representative localities (i.e., P1 and P3 in a) of the initial model are shown at the right. (c) Illustrations of the mechanical and thermal boundary conditions used in the model. (For interpretation of the references to color in this figure legend, the reader is referred to the web version of this article.)

geological data, which indicate that the southern Asian margin may have established a thicker and weaker crust than that of the cratonic Indian plate before the India-Asia collision (e.g., Murphy et al., 1997; Kapp et al., 2005; Ding et al., 2014). Its crust is initially composed of a 30 km-thick upper crust and a 20 km-thick lower crust, which rests on a 50 km-thick lithospheric mantle and a ~83 km-thick asthenosphere. A relatively cold continental lithosphere is prescribed for the rest of the model domain, simulating the normal continent surrounding the proto-plateau, also known as retro-lithosphere. Its crust is initially composed of a 15 km-thick upper crust and a 25 km-thick lower crust, which overlies an 80 km-thick lithospheric mantle and a 60 km-thick asthenosphere. The continental upper crust has a uniform radiogenic heat production of 1.2 μW/m^3, which is three times higher than that in the lower crust (0.4 μW/m^3). This configuration self-consistently produces a proto-plateau with an elevation of 2.5 km and surface heat flow of ~60 mW/m^2, surrounding by a continent with an elevation of 0 km and surface heat flow of ~46 mW/m^2 (Fig. 1a). Note that there is a large uncertainty about radiogenic heat production in the continental crust (e.g., Clark et al., 2011; Furlong and Chapman, 2013). Tests show that the use of other values (1.0 or 1.5 μW/m^3) for the upper crust does not affect the overall model behavior. The lateral variations in initial crustal thickness and thermal state result in that the viscosity of the plateau crust is about 2 orders of magnitude lower than that of the surrounding continent (Fig. 1b). Thus, our model setup implicitly introduces lateral strength heterogeneity for the two colliding continental lithospheres. The initial rheological heterogeneity is prescribed to capture the tectonic inheritance of the upper plate resulted from pre-collision oceanic subduction or continental block amalgamation (e.g., Yin and Harrison, 2000).

In the modeling, we assume that the continental upper crust has a felsic composition, which is represented by the 'wet quartzite' flow law (Ranalli, 1995) and the 'granite' solidus and liquidus (Johannes, 1985; Poli and Schmidt, 2002), whereas the continental lower crust has a mafic composition, which is represented by the 'plagioclase An$_{75}$' flow law (Ranalli, 1995) and the 'tholeitic basalt' solidus and liquidus (Hess, 1989). This assumption is in reasonable agreement with our understanding of the composition and nature of the continental crust (e.g., Hacker et al., 2015; Rudnick and Fountain, 1995; Rudnick and Gao, 2014). The lithospheric and asthenospheric mantle is characterized by the flow law of 'dry olivine' and the melting regime of 'peridotite' (Katz

Table 1
Thermal properties used in the numerical experiments.[a]

Rock type	ρ_0, kg/m^3	Thermal conductivity W/(m K)	$T_{solidus}$ K	$T_{liquidus}$ K	Latent heat kJ/kg	Heat production μW/m^3
UCC	2700 (solid) 2400 (molten)	(0.64 + 807/(T + 77))	889 + 17,900/(P + 54) + 20,200/(P + 54)^2 at $P < 1200$ MPa, 831 + 0.06P at $P > 1200$ MPa	1262 + 0.09P	300	1.2
LCC	2800 (solid) 2500 (molten)	(1.18 + 474/(T + 77))	1327.15 + 0.0906P	1423 + 0.105P	380	0.4
LAM	3300 (solid) 2700 (molten)	(0.73 + 1293/(T + 77)) × (1 + 0.00004P)	Melting model of Katz et al. (2003)	Melting model of Katz et al. (2003)	400	0.022
References	1, 2	3	4–8	4, 8	1, 2	–

[a] T is temperature in Kelvin, and P is pressure in MPa. UCC, upper continental crust; LCC, lower continental crust; LAM, lithospheric/asthenopsheric mantle. 1 = Turcotte and Schubert, 2002; 2 = Bittner and Schmeling, 1995; 3 = Clauser and Huenges, 1995; 4 = Schmidt and Poli, 1998; 5 = Hess, 1989; 6 = Hirschmann, 2000; 7 = Johannes, 1985; 8 = Poli and Schmidt, 2002. Other properties (for all rock types): C_p = 1000 J kg^{-1} K^{-1}, $\rho = \rho_0[1 - \alpha(T - T_0)] \times [1 + \beta(P - P_0)]$, where $\alpha = 3 \times 10^{-5}$ K^{-1} is thermal expansion and $\beta = 1 \times 10^{-5}$ MPa^{-1} is compressibility; ρ_0 is density at room condition (T_0 = 298 K and P_0 = 0.1 MPa).

et al., 2003). The latter is characterized by a lower geothermal gradient (~0.5°C/km) and convective heat transfer, whereas the former is characterized by a higher geothermal gradient and conductive heat transfer. The primary thermal parameters used here are listed in Table 1. More details on the methods and parameters can be found in Chen and Gerya (2016).

In the rest of the paper, we refer to boundaries of our models in terms of geographic designations. The south boundary corresponds to the front wall where the convergence operates.

3. Modeling results

We performed 6 numerical experiments to explore the effects of convergence rate, radioactive heating, shear heating, and basal heating on mid-crustal melting during collisional orogenesis (Table 2). We chose the model, which has a pre-thickened and hot active margin, a convergence rate (V_c) of 3.3 cm/yr and non-zero radiogenic heat production (Model 1 in Table 2), as the reference model. A convergence rate of 3.3 cm/yr used here is in agreement with the estimate of 3.5 ± 1.3 cm/yr for Cenozoic Asian shortening rate by Guillot et al. (2003).

3.1. The reference model

In order to provide context for various tests and enable direct comparison to our previous study (Chen and Gerya, 2016), we first describe the results of the reference model. Fig. 2 shows that an orogenic plateau progressively develops on the framework of the pre-weakened margin as convergence continues, which is similar to those observed in our previous study (Chen and Gerya, 2016). After several hundreds of kilometers of convergence, the plateau crust is thickened to ~65 km and the thickened upper crust starts to melt (Fig. 2a, b). Considerable intracrustal melting occurs at the later stage of the model, when crustal thickening enforces the considerable volumes of the lowermost upper crust to come across the isotherm of 600°C (Fig. 2c). Thus, the crustal melting occurs at the bottom of the thickened upper crust, forming a mid-crustal partial melting layer embedded in the transition between the upper and lower crust (the red in Fig. 2b, c; see the material codes in Fig. 1). It is the partially molten phase of the upper crust. Therefore, the mid-crustal melting observed here is a product of in situ partial melting of the deep-seated felsic rocks during crustal thickening. With continued convergence, the mid-crustal melting layer migrates towards north and east (Fig. 3i). This accompanies the northward and eastward crustal heating, and eventually leads to the melt-weakening of the plateau crust (Fig. 3ii–iii). The constant convergence together with melt-weakening creates a large flat orogenic plateau over the region of the thickened crust (Fig. 2c). Note our model predicts no melting of the lower crust even at the later stage. This is because the mafic nature of the lower crust makes it refractory to in situ melting.

3.2. Effect of convergence rate

This set of models (Models 1–3 in Table 2) was designed to examine the influence of convergence rate on the development of orogenic plateau and crustal melting. The Model 2 and 3 are identical to the reference model, except that the convergence rates applied to them are 1.5 and 5.0 cm/yr, respectively, instead of 3.3 cm/yr in the reference model. Fig. 4 shows the snapshots as well as horizontal slices (Y = 50 km) resulted from these models, which are produced after the same amount of convergence (ca. 1000 km). Note that Y = 50 km corresponds to the real depth of 34–38 km (the same below). In these cases, there are no significant differences in the resultant orogenic plateau and lithospheric architecture. However, the extent of mid-crustal melting depends highly on the convergence rate. For a slow convergence rate (e.g., V_c = 1.5 cm/yr; see Fig. 4a), the thickness of

Table 2
Conditions and results of 3d numerical experiments.[a]

Model name	V_c (cm/yr)	Radioactive heating	Shear heating	Basal heating	Figures	Comments
Model 1 (reference)	3.3	Yes	Yes	No	1–4, 9–11	Crustal melting
Model 2	1.5	Yes	Yes	No	4	Crustal melting (thick)
Model 3	5.0	Yes	Yes	No	4	Crustal melting (thin)
Model 4	3.3	No	Yes	No	5	No crustal melting
Model 5	3.3	Yes	No	No	5	Crustal melting (thin)
Model 6	3.3	Yes	Yes	Yes	6–8	Crustal melting (thick)

[a] V_c, convergence rate.

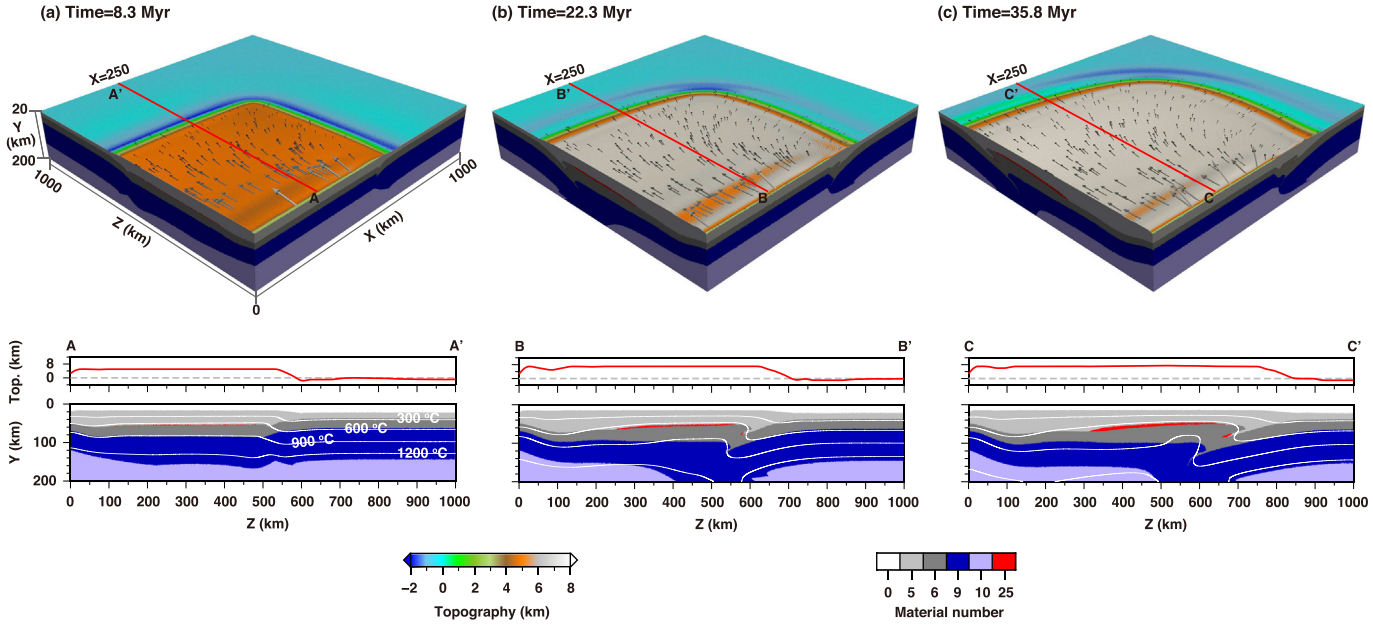

Fig. 2. Reference model showing the growth of an orogenic plateau from a cold small one to a large hot one. Top row: snapshots of 3-D model showing lithospheric deformation and surface topography at **a** 8.3, **b** 22.3, and **c** 35.8 Myr. The labeled time is from the start of the simulation (the same below). The colors and arrows on the top of the models indicate the topography and the local surface velocity, respectively. Bottom row: cross-sections of material field and topography along the middle of the plateau (AA′, BB′, CC′). The white lines are isotherms at intervals of 300°C. The color codes for topography and material are shown at the bottom of the figure (see Fig. 1 for details). (For interpretation of the references to color in this figure legend, the reader is referred to the web version of this article.)

mid-crustal partial melting layer can be up to 15 km, and the melting layer covers most of the area of the plateau (Fig. 4i–ii). Long-standing heating, including radioactive heating and shear heating, during crustal thickening causes the plateau middle crust to become rather hot (600–700 °C) and weak (Fig. 4iii–iv). This eventually leads to the southward flow of the melt-weakened middle crust at the southeastern edge of the model, where the direction of motion is opposite to convergence. For an intermediate convergence rate (e.g., $V_c = 3.3$ cm/yr; see Fig. 4b), this layer can be up to 10 km thick and covers the northern half of the plateau's area. In the case of fast convergence (i.e., $V_c = 5.0$ cm/yr; see Fig. 4c), the thickness of mid-crustal melting layer is < 5 km and the melt region only occupies one third of the plateau's area. This is because faster convergence causes the thickened crust to have less time for radioactive heating.

3.3. Effect of radioactive heating

As mentioned above, radiogenic heat production is a critical heat source for crustal melting during collisional orogenic process (e.g., Jamieson et al., 1998; Beaumont et al., 2004; Faccenda et al., 2008). To examine the effect of radioactive heating on the development of mid-crustal melting in depth, we performed simulations on 'Model 4' (see Table 2). This model differs from the reference model in that radiogenic heat production is set to zero for all the rocks. In this case, the resultant orogenic plateau and lithospheric structure are similar to those observed in the reference model at the equivalent time step (Fig. 5a). Relative to the reference model (Fig. 2), the convergence here is accommodated more by crustal thickening and less by outward expansion. This leads to extremely thick crust beneath the plateau, and causes the amount of the outward expansion along the northern plateau margin to be ca. 100 km less than that of the reference model after ~36 Myr of convergence (Fig. 5ai). The overthickened plateau crust bends the surrounding lithosphere and creates a foreland basin rimming the plateau, which is not notable in other models. Despite huge thickness of the plateau crust, its thermal state is rather cold. For example, the crust temperature at Y = 50 km under the plateau is overall no > 450°C (Fig. 5aii). Therefore, no crustal melting occurs within the plateau crust even at the later stage owing to the absence of radioactive heating in this model. In this case, the cold plateau crust sustains relatively high viscosity throughout the model evolution (Fig. 5aiii). This explains in part the less outward growth of the plateau. The comparison between this model and the reference model highlights the importance of radioactive heating in generating mid-crustal partial melting during collisional orogeny, which is discussed further in Section 4.

3.4. Effect of shear heating

Shear heating has been shown to be another important heat source during continental collision (England and Molnar, 1993; Burg and Gerya, 2005; Nabelek et al., 2010). To examine its role in crustal

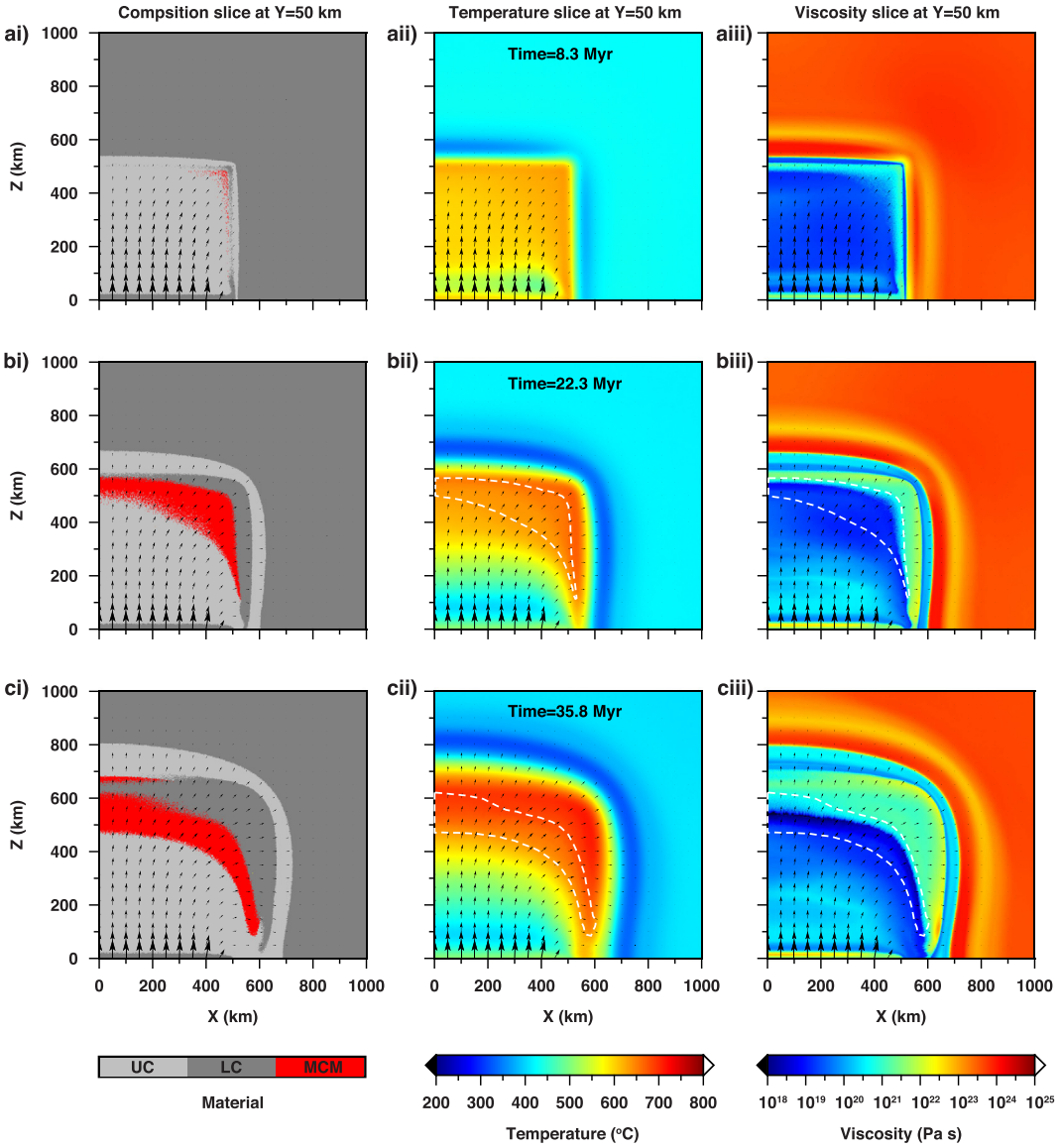

Fig. 3. Horizontal slices of material, temperature and viscosity for the reference model. The slices roughly cross the center of the mid-crustal melting layer at Y = 50 km, which corresponds to the real depth of 34–38 km (the same below). **i**, material slices with the model time **a** 8.3, **b** 22.3, and **c** 35.8 Myr. **ii**, temperature slices. **iii**, viscosity slices. The dashed white lines encompass the main areas of mid-crustal melting (the same below). UC, upper crust; LC, lower crust; MCM, mid-crustal melt, which are the same for all the following figures.

melting during the evolution of orogenic plateau, we conduct the experiment 'Model 5' (see Table 2). This model is identical to the reference model, except that the function of shear heating is excluded. Fig. 5b shows the snapshot and horizontal slices of the model absent of shear heating. Again, the results are similar to those observed in the reference model at the equivalent time step. Notable differences are manifested in the following two aspects. First, the thickness or the area of the mid-crustal melting layer is much less than that in the reference model. Second, the plateau forces the surrounding lithosphere to be bent more than that of the reference model, which is accompanied by less overthrusting of the plateau margin onto the surrounding continent (Fig. 5b). This is because exclusion of shear heating reduces the internal heat source in the thickened plateau crust and, to some extent, increases its strength. The comparison of the model without shear heating and the reference model shows that shear heating is an important factor in shaping the deformation style during collisional orogeny. However, the experiments evidently demonstrate that the role of shear heating in mid-crustal melting is secondary to radioactive heating.

3.5. *Effect of basal heating*

Basal heating, which can be resulted from asthenosphere upwelling due to slab breakoff or lithosphere delamination (e.g., Bird, 1979; Davies and von Blanckenburg, 1995; Jimenez-Munt and Platt, 2006), is another important heat source during collisional orogeny. To investigate the effects of basal heating on crustal melting, we performed the simulation of 'Model 6' (see Table 2). For simplicity, we remove the lithospheric mantle under the region of $0 \le x \le 400$ km and $100 \le z \le 400$ km from the beginning and keep the rest of parameters the same as the reference model in this model. This creates an asthenosphere window beneath the central part of the proto-plateau (Fig. 6a), mimicking a sudden removal of the plateau lithosphere mantle due to delamination or foundering (e.g., Bird, 1979; Kay and Kay, 1993). The replacement of cold lithosphere mantle with hot asthenosphere leads to basal heating of the plateau crust and decompression melting of the gap-filling asthenasphere (i.e., the orange material in Fig. 6). The asthenospheric melting disappears within ~5 Myr of the onset of convergence as the newly-added heat is transferred

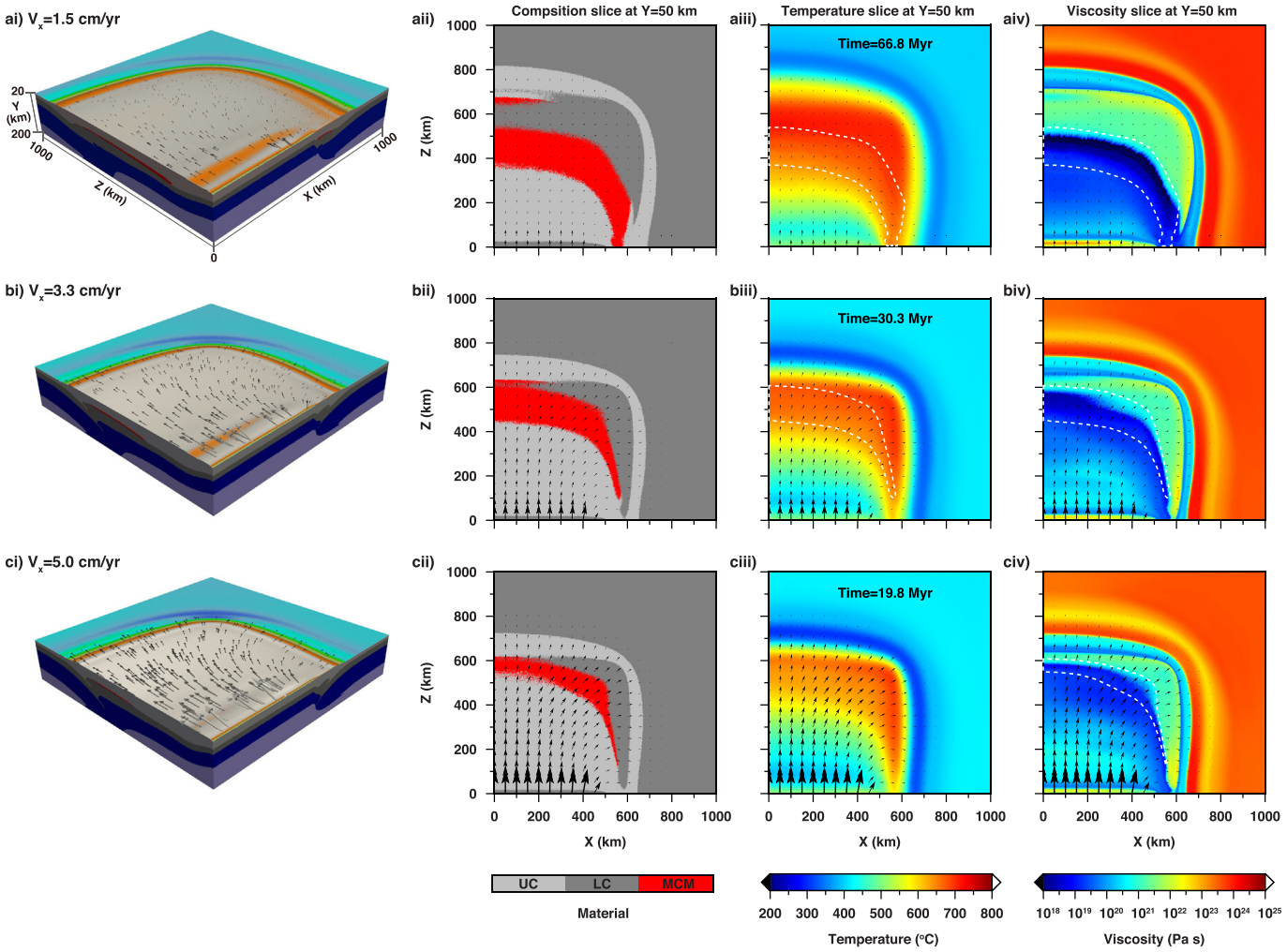

Fig. 4. Influence of convergence rate on orogenic plateau growth and mid-crustal melting. **i**, snapshots of 3-D models showing lithospheric deformation and surface topography with convergence rate characterized by **a** 1.5, **b** 3.3, and **c** 5.0 cm/yr. **ii**, material slices at Y = 50 km. **iii**, temperature slices at Y = 50 km. **iv**, viscosity slices at Y = 50 km. The snapshot for each model corresponds to the equivalent amount of bulk convergence (~1000 km): **a)** Model 2 at 66.8 Myr; **b)** Model 1 (the reference model) at 30.3 Myr; **c)** Model 3 at 19.8 Myr. The color codes for topography and material can be found in Fig. 1.

towards the surrounding cold area by convergence-driven advection (Fig. 7). Heating the plateau crust from below strongly decreases the strength of the plateau lithosphere and allows faster northward underthrusting of the cold pro-lithosphere coming from the south (Fig. 8). After ~23 Myr of convergence, the asthenosphere window is closed. In the context of convergence, heat carried by the asthenosphere window is more efficiently transferred to the surrounding lithosphere, in particular to the northern and eastern margins of the plateau, than to the overlying crust (Fig. 7). This leads to overall temperature elevation of the model crust by a few tens to one hundred degrees relative to the reference model (Fig. S3), and distributed uplift of the surrounding continent. and a limited increase of mid-crustal melting relative to the reference model (Fig. 6b–d). In contrast to the reference model, the resulting mid-crustal melting layer at the later stage is a few kilometers thicker (Fig. S4), but the architecture of the resulting orogenic plateau is quite similar. We conclude that basal heating through slab breakoff or delamination during collisional orogeny plays an important role in the regional temperature increase and surface uplift and a relevant role in promoting mid-crustal melting. Note that if basal heating is triggered after the establishment of a large hot plateau, its contribution to crustal melting should be more significant.

4. Discussion

Results presented in Section 3 provide a description of the main physical processes accompanying the formation of orogenic plateau and on how these processes can be affected by different combinations of model parameters. In this section, we discuss the conditions and consequences of the presence of mid-crustal melting and relate the results to the crustal deformation behavior beneath the Tibetan plateau.

4.1. Physical controls for intra-crustal melting

Mid-crustal partial melting (i.e., in situ crustal melting) has been repeatedly observed in the models presented above. Here we explore the physical controls for its generation. Fig. 9 shows the temporal evolution of temperature, temperature gradient and viscosity profiles at the site P2 (X = 250 km and Z = 400 km; see Fig. 1) for the reference model. At the onset of convergence, the overall temperature of the upper crust (i.e., the portion above the blue dashed line in Fig. 9a) is below the granite solidus (Johannes, 1985; Poli and Schmidt, 2002), and there is no clear dividing line on the temperature gradient curve between the upper and lower crusts. At the later stage, the temperature at the lowermost portion of the upper crust exceeds the granite solidus (red curve in Fig. 9a), which triggers in situ partial melting. The temperature gradient of the upper crust is several times higher than that of

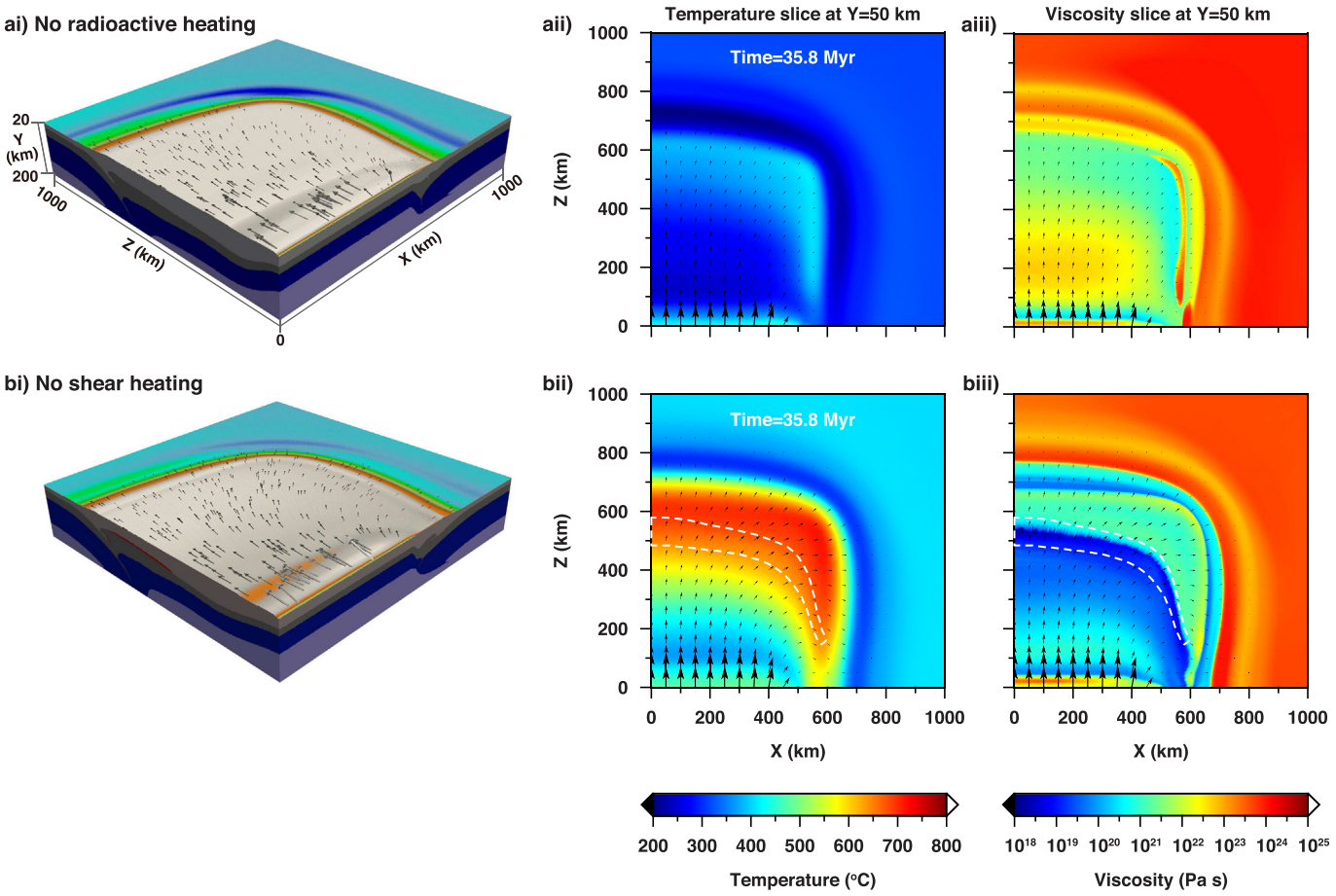

Fig. 5. Influence of radioactive heating and shear heating on orogenic plateau growth and mid-crustal melting. **i**, snapshots of 3-D models showing lithospheric deformation and surface topography without **a** radioactive heating (Model 4) and **b** shear heating (Model 5), in contrast to the reference model. **ii**, temperature slices at Y = 50 km. **iii**, viscosity slices at Y = 50 km. For the purpose of comparison, the chosen model times for the snapshots are identical to that in Figs. 2c and 3c. The color codes for topography and material can be found in Fig. 1.

the sub-upper crust (i.e., the portion beneath the upper crust). This is because the radiogenic heat production of felsic rocks (upper crust) is several times (three times here; see Table 1) greater than that of mafic rocks (lower crust) (e.g., Furlong and Chapman, 2013), and the effect of this contrast is amplified as cumulative time increases. Convergence-driven crustal thickening steepens the geothermal boundary between the upper and lower crust and eventually leads to an upper crust-dominant geothermal gradient and melt weakening (Fig. 9b,c). This implicates that the temperature increase in the upper crust is much faster (3–4 times) than that in the lower crust and lithosphere mantle. The transition of the thermal regime reflects the nature of the compositional difference (e.g., radiogenic element content) between the upper crust and lower crust during crustal thickening (e.g., McKenzie and Priestley, 2008; Furlong and Chapman, 2013; Hacker et al., 2015).

Our results presented above have demonstrated that when the effect of radioactive heating is excluded, no crustal melting occurs at all. Mid-crustal melting predicted in the reference model is generated by tectonically driven crustal self-heating (i.e., radioactive/shear heating). This is consistent with the analyses by Medvedev and Beaumont (2006), showing that high values of radioactivity and low values of thermal capacity for the upper crust can produce temperatures compatible with the onset of melting.

Basal heating due to slab breakoff or convective removal of the lithospheric mantle (e.g., Davies and von Blanckenburg, 1995; Houseman and Molnar, 2001; Molnar et al., 1993), as shown in Model 6, produces a broad-area increase of the crust temperature and surface topography and promotes the thickness of mid-crustal melt layer. In the setting of intense convergence, the horizontal thermal advection plays a more prominent role in the redistribution of the newly-added heat than the thermal conduction. This explains the vast area of the temperature elevation and surface uplift and the relatively limited increase of crustal melting. On one hand, this simulation indicates that both the orogen-perpendicular and orogen-parallel transports of material and heat are important processes during orogeny, which cannot be ignored. On the other hand, this also demonstrates that our understandings on orogens from 2D models may be incomplete, because 2D models are incapable of modeling the orogen-parallel processes. The latent heat associated with melting is another heat source, which is also considered in our models (see Table 1). It can supply heat to sustain partial melting as melt crystallizes, but it cannot contribute to initiate and facilitate crustal melting. We conclude that crustal thickening-assisted radioactive heating during orogeny is the dominant mechanism for deep crustal melting.

Fig. 10 shows the evolution of shear heating as well as the second strain rate invariant during the growth of orogenic plateau in the reference model. The region with high shear heat is mainly concentrated in the region where significant mantle thickening occurs or at the plateau margin, in particular at the later stage. This is resulted from fast deformation of the plateau mantle as lithospheric thickening and high localized strain beneath the plateau margin owing to overthrusting of the plateau crust onto the surrounding continent as the plateau grows outward. The magnitude of shear heat production is up to 0.1 to > 1 $\mu W/m^3$, which is comparable to radiogenic heat production within the upper crust (Table 1). The heat source generated by shear deformation

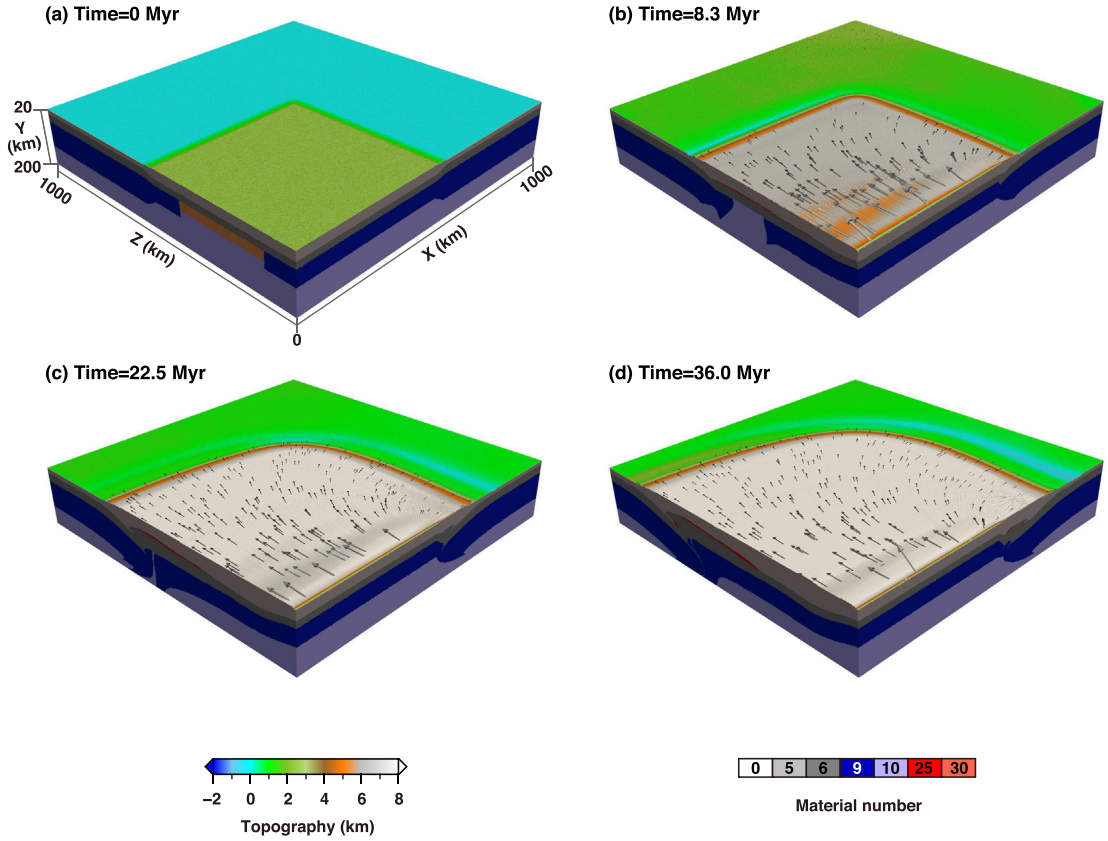

Fig. 6. Influence of basal heating on orogenic plateau growth and mid-crustal melting. The snapshots show the evolution of a proto-plateau, which is absent of lithospheric mantle under the central region of the model (Model 6): **(a)** Time = 0 Myr; **(b)** Time = 8.3 Myr; **(c)** Time = 22.5 Myr; **(d)** Time = 36.0 Myr. Note the orange material shown in **(a)** represents decompression melting of the asthenosphere. The color codes for topography and material are shown at the bottom of the figure (see Fig. 1 for details). (For interpretation of the references to color in this figure legend, the reader is referred to the web version of this article.)

may be transferred to the overlying crust through thermal conduction (e.g., Burg and Gerya, 2005). Thus, shear heating, as an additional source of energy during collisional orogeny, facilitates the development of mid-crustal melting, but its role is secondary to radioactive heating as shown in the above simulations.

In summary, redistribution of crustal material during convergence increases crustal heat production in the growing orogenic plateau, leading to T ≥ 600°C in substantial volumes of the middle and lower crust after ~20 Myr since the onset of convergence. It is the inherent contrast in the abundance of radiogenic elements (U, Th, K) between the felsic upper crust and mafic lower crust that makes the lowermost portion of the upper crust favorable for generating in situ partial melting. The increasing and accumulating radioactive and shear heating during convergence-driven crustal thickening provides the heat source needed for mid-crustal melting.

4.2. Consequences of mid-crustal melting

A number of studies have indicated that the occurrence of in situ crustal melting can lead to a dramatic reduction in crustal strength (e.g., Arzi, 1978; Beaumont et al., 2004; Brown, 2007; Jamieson et al., 2011; Rosenberg and Handy, 2005). In fact, Fig. 9c shows that melt-induced reduction in viscosity can be up to one order of magnitude, which is consistent with the inference that in situ melt-weakening amounts to approximately a factor of 10 decrease in effective viscosity (Beaumont et al., 2004). Below we provide an in-depth analysis of the consequences of mid-crustal melting in crustal deformation behavior.

The reduction of viscosity within the partial melting layer has the potential for mechanical decoupling between the overlying upper crust and underlying lower crust. Fig. 11 shows two cross-sections of the second strain rate invariant as well as the velocity field for the reference model at 42.3 Myr. The mid-crustal melting zone is characterized by remarkably higher strain rate relative to its overlying and underlying region (Fig. 11c, d), reflecting faster localized strain there. The apparently larger magnitude of the Z- and X-components of the velocity in the mid-crustal melting zone indicates that this layer flows both northward and eastward relative to its surrounding region (Fig. 11e, f). This therefore demonstrates that the upper crust is decoupled from the lower crust and lithospheric mantle due to the presence of the mid-crustal melting layer.

Therefore, our model results provide convincing evidence for crustal decoupling due to mid-crustal partial melting. Mechanical decoupling occurs preferentially at mid-crust depth beneath the mature orogenic plateau in response to melt-weakened effect. The partial melting layer decouples from its overlying and underlying crust by eastward and northward dominant flow. This implies that the mid-crustal melting eventually induces a localized crustal flow channel, which transports partially molten material from beneath the plateau interior towards its eastern and northern margin driven by the combination of the north-south compression and the pressure gradient. Note that our models predict that the crustal flow occurs only at the later stage of orogenic plateau evolution and, significantly, it is confined to a thin layer at the mid-crustal level, rather than in the lower crust as the crustal channel flow model argued (e.g., Beaumont et al., 2004; Royden et al. 1997, 2008).

4.3. Implications for crustal deformation at the Tibetan plateau

Geophysical data show that the mid- to lower crust beneath the Tibetan plateau is characterized by low seismic velocity or low

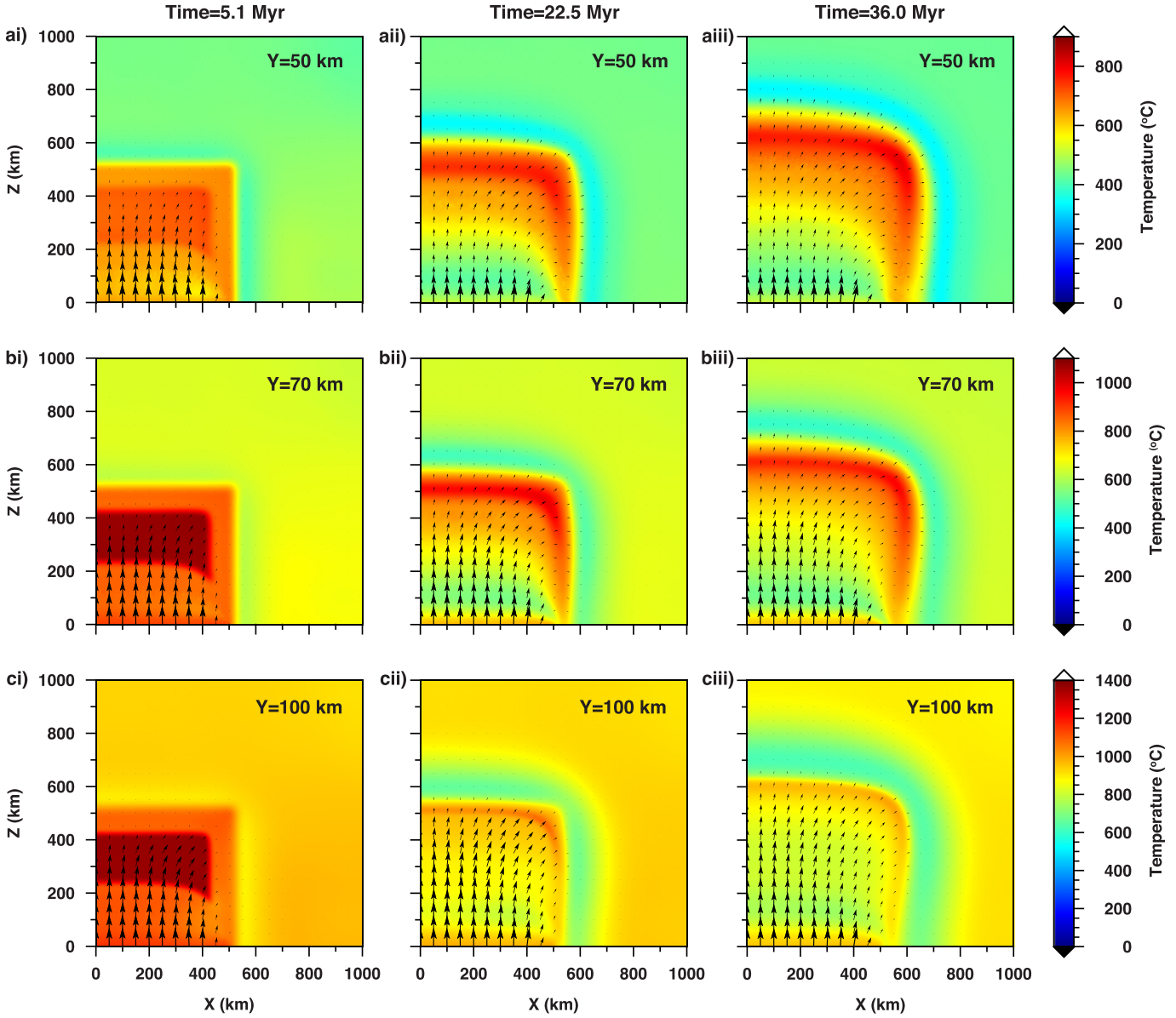

Fig. 7. Thermal evolution of the model with basal heating. Horizontal slices show the temperature distribution at various depths and times when the model is subjected to basal heating. **i**, temperature distribution at 5.1 Myr with **a** Y = 50 (middle crust depth), **b** Y = 70 (lower crust depth), and **c** Y = 100 km (lithosphere mantle or asthenosphere depth). **ii**, temperature distribution at 22.5 Myr. **iii**, temperature distribution at 36.0 Myr. Note that the heat input through basal heating is quickly transferred towards the plateau margins, in particular the northern margin, because of convergence.

resistivity (e.g., Bai et al., 2010; Bao et al., 2015; Unsworth et al., 2005; Yang et al., 2012). For example, recent seismic ambient noise data reveal that inter-connected low shear velocity zones distribute across most of the Tibetan middle crust at depths between 20 and 40 km and they are most prominent in the periphery of Tibet (e.g., Yang et al., 2012; Bao et al., 2015). However, the cause for these low velocity or resistivity zones remains controversial. The proposed explanations include preferred orientation of micas, the presence of aqueous fluids, crustal shearing, and crustal partial melting, etc. (e.g., Wei et al., 2001; Vergne et al., 2002; Shapiro et al., 2004; Klemperer, 2006). Meanwhile, petrological data from scattered localities, in particular at rifts or grabens, provide convincing magmatic evidence for crustal melting under the Tibetan plateau (e.g., Chung et al., 2003, 2005; Ding et al., 2003; Hacker et al., 2000; Wang et al., 2012). For example, the High Himalayan leucogranites represents the exposure of such deeply-seated crustal melting (e.g., Beaumont et al., 2001; Cottle et al., 2015; Harris, 2007). The exposures of igneous rocks aging from Eocene to Quaternary have also been documented in central and northern Tibet (e.g., Hacker et al., 2000; Wang et al., 2010, 2012). How are the geophysical data reconciled with the petrological data? If the mid-crustal melting exists, whether is it pervasive throughout the Tibetan plateau or restricted to the rifts? When did the plateau crust start to melt? These questions are still open.

Our 3-D models show that mid-crustal melting is a product of the combination of self-heating (radioactive/shear heating) accompanying crustal thickening and compositional contrast between the upper and lower crust. It emerges after ~20 Myr of convergence, and accumulates at the base of the thickened upper crust. This is in agreement with the above-mentioned petrological data, which indicate a long-lived history of crustal melting beneath the Tibetan plateau (e.g., Wang et al., 2010, 2012). The mid-crustal depth of crustal melting predicted by our models is consistent with the depths of 20–40 km for the low velocity or resistivity zones in Tibet (Bai et al., 2010; Bao et al., 2015; Unsworth et al., 2005; Yang et al., 2012). At the later stage, the areas with the

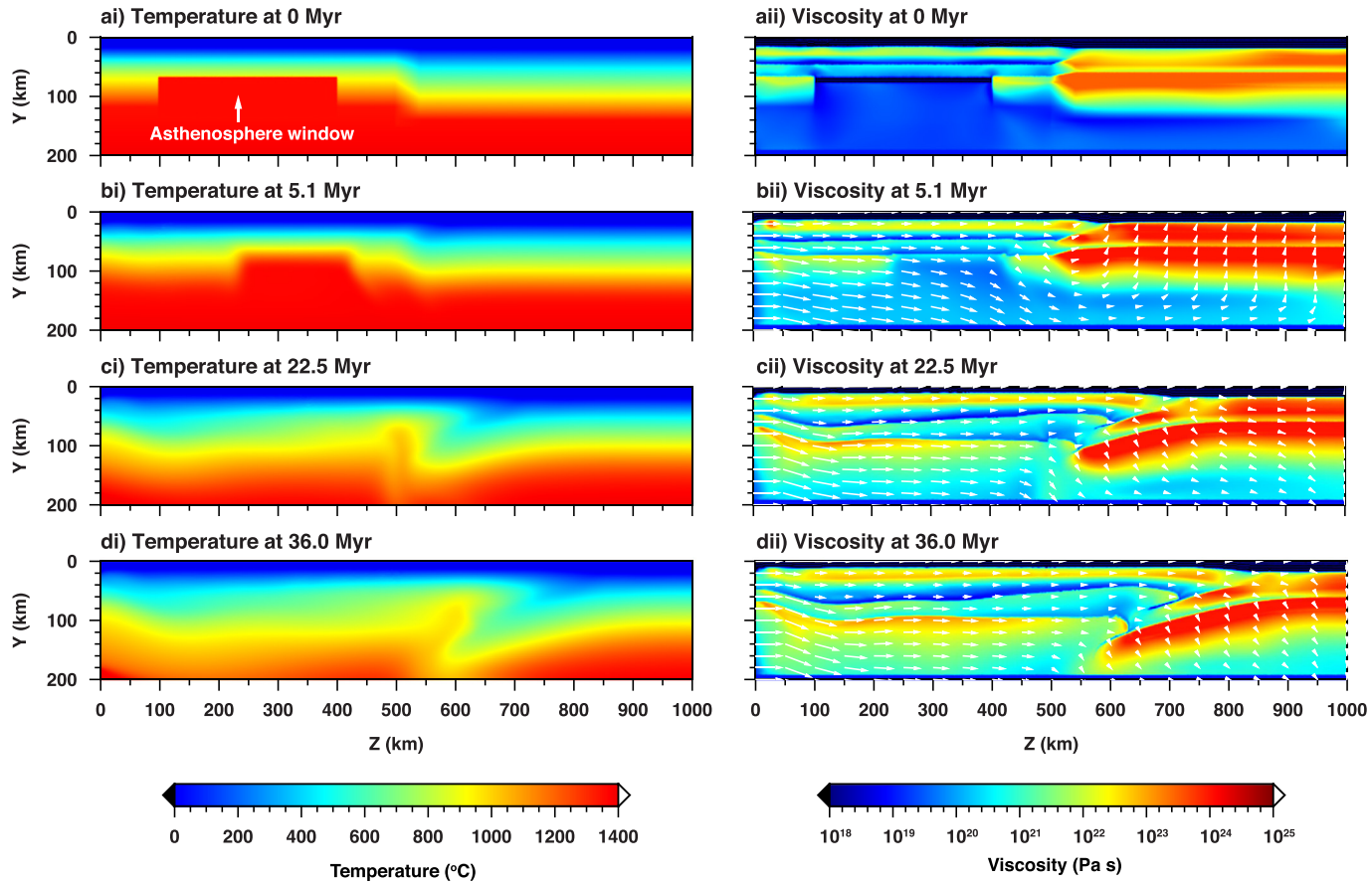

Fig. 8. Thermal-rheological consequences of basal heating. Cross-sections show the evolution of the temperature and viscosity fields with time when an asthenosphere window is created beneath the plateau at the beginning of simulation. **i**, the cross-section of the temperate field along X = 250 km (see the yellow line in Fig. 1a) at **a** 0, **b** 5.1, **c** 22.5, and **d** 36.0 Myr. **ii**, the cross-sections of the viscosity field along X = 250 km at different times. The white arrows indicate the velocity vectors showing the direction of material motion.

mid-crustal melting become interconnected and widespread under the central and northern plateau. The present-day Tibetan plateau is a typical large hot orogenic plateau (Jamieson and Beaumont, 2013), just like the later-stage plateaus presented here. Thus, we suggest that the mid-crustal melting is pervasive beneath the Tibetan plateau, and it is the cause leading to widespread low velocity or resistivity zones within the plateau crust as revealed by geophysical data. Scattered felsic igneous rocks exposed at the extensional rifts or large-scale faults are likely the surficial expression of the widespread mid-crustal melting, because crustal-scale faults can provide outlets for exposures of the deep crustal melt. The continued north-south convergence together with the increasing potential gravitational energy drives the mid-crustal partial melt to flow towards north and predominantly towards east. Apparently, such a consistent outward flow would lead to the marginal dominance of the mid-crustal partial melt. Therefore, our results also provide a self-consistent explanation for the periphery-dominant low shear velocity features in northern Tibet observed on recent seismic data (Yang et al., 2012; Bao et al., 2015).

The presence of mid-crustal melting in our models postdates the formation of a large and broad orogenic plateau, thus it is not the cause responsible for the plateau formation. The outward flow of partially molten mid-crust materials at the later stage is also limited in volume, thus is not the primary cause for the outward growth of the plateau at its margins, unlike previously proposed and inferred (Clark and Royden, 2000; Royden et al., 1997). However, its occurrence results in dramatic reduction of crustal strength and leads to mechanical decoupling between the overlying upper crust and underlying lower crust. The mid-crustal melting layer flows eastward relative to its upper and lower boundary. This confirms that the melt-weakened middle portion of the thickened crust is capable of flow in channel (e.g., Beaumont et al., 2001, 2004; Clark and Royden, 2000; Royden et al., 1997). The generation of a partially molten mid-crustal layer functions as a lubricant to facilitate lateral crustal ductile flow, and has profound effect on the plateau evolution at the later stage. For example, it may limit crustal thickness of the plateau, flatten the plateau surface and trigger orogen-parallel extension and eventual collapse of the plateau.

5. Model limitations

In order to better concentrate on the factors controlling deep crustal melting, here we do not model the surface processes, such as erosion and sedimentation. Jamieson and Beaumont (2013) have demonstrated that increased erosion rates in the Himalaya may be responsible for reactivating the Main Central Thrust using dynamical models. The response of orogens to climate-driven enhanced erosion includes a decrease in the width of the orogenic belt, a short-term increase in sediment yield, a persistent increase in the rate of rock exhumation, and a reduction in the subsidence of adjacent foreland basins (e.g., Whipple, 2009). Furthermore, focused erosion only has a significant impact on the steep slopes of orogens, and its effect on the vast plateau interior is limited (e.g., Beaumont et al., 2004). Thus, it can be envisaged that if erosion is considered here, more material at the plateau margins will be transported to the adjacent foreland basins and more metamorphic or igneous rocks will be exhumed at the plateau margins. Its effect on the occurrence of mid-crustal melting beneath the plateau may be limited.

The melt transport process and melt reactions are not incorporated

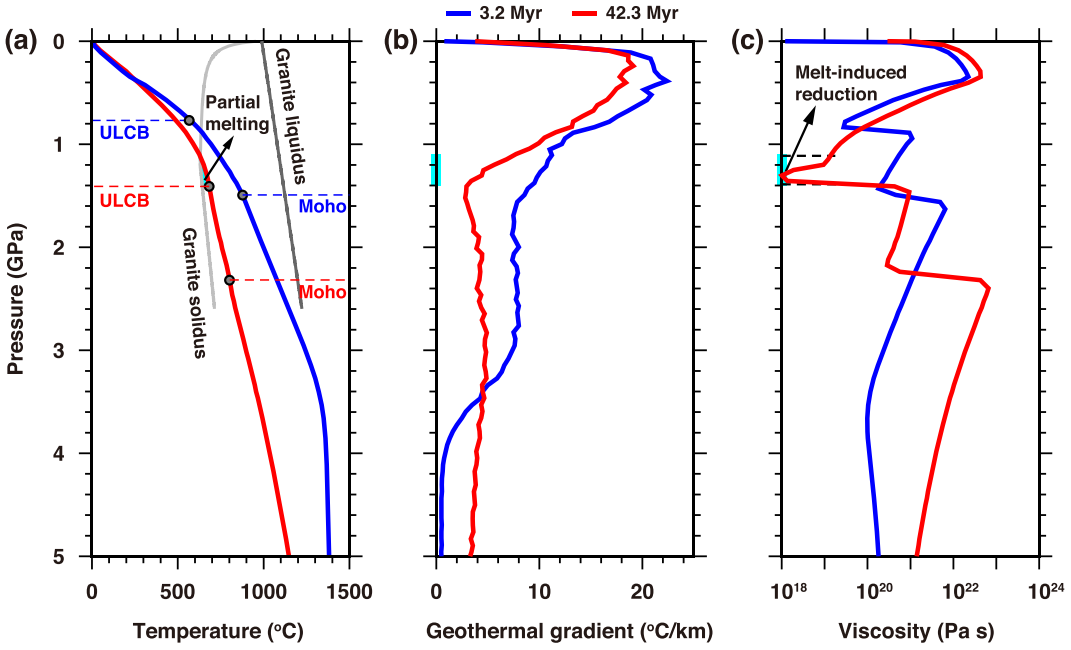

Fig. 9. Illustration of mid-crustal partial melting and its consequence in viscosity. The results are for the reference model at fixed point P2 (i.e., X = 250 and Z = 400 km; see Fig. 1 for the position). (a) Temperature profiles and granite solidus and liquidus, showing the condition of partial melting; (b) profiles of temperature gradient; and (c) viscosity profiles. Cyan-filled region indicate the region where crustal partial melting occurred at 42.3 Myr. Blue and red dashed lines indicate the bottom of upper crust at 3.2 and 42.3 Myr, respectively. ULCB, upper-lower crustal boundary, below which the granite solidus and liquidus are not applicable as the composition changes into the lower crust or mantle. (For interpretation of the references to color in this figure legend, the reader is referred to the web version of this article.)

in our modeling as well. Numerical modeling of melt transport involves the theories of two-phase flow, melt segregation, melt extraction etc. (e.g., Keller et al., 2013; Cao et al., 2016), which is beyond the scope of this study. It is noteworthy that efficient melt transport driven either by pressure gradients or crustal shearing will reduce the melt fraction. This likely leads to overestimates of the melt-weakened effect of the molten rocks and underestimates of the volume of rocks affected by melt in our models. In addition, as partially molten material migrates up, it should take the heat. When the melt crystallizes, the melt zone should broaden over time. In view of this, our model results likely underestimate the region which is affected by mid-crustal melting.

For simplicity, the asthenosphere window is created at the beginning of the simulation with basal heating (i.e., Model 6). A more realistic case is that the asthenosphere window forms after the establishment of a large orogenic plateau, when the plateau crust/lithosphere becomes thick enough to initiate convective removal (e.g., Molnar et al., 1993). Such a process is not modeled here due to the operative complexity. For example, both the compositional and thermal structures become heterogeneous in the middle of simulation, which makes human intervention difficult. Based on the model results from Model 6, we infer that if basal heating operates at the later stage of the model, there is likely to be more partial melting within the plateau's middle

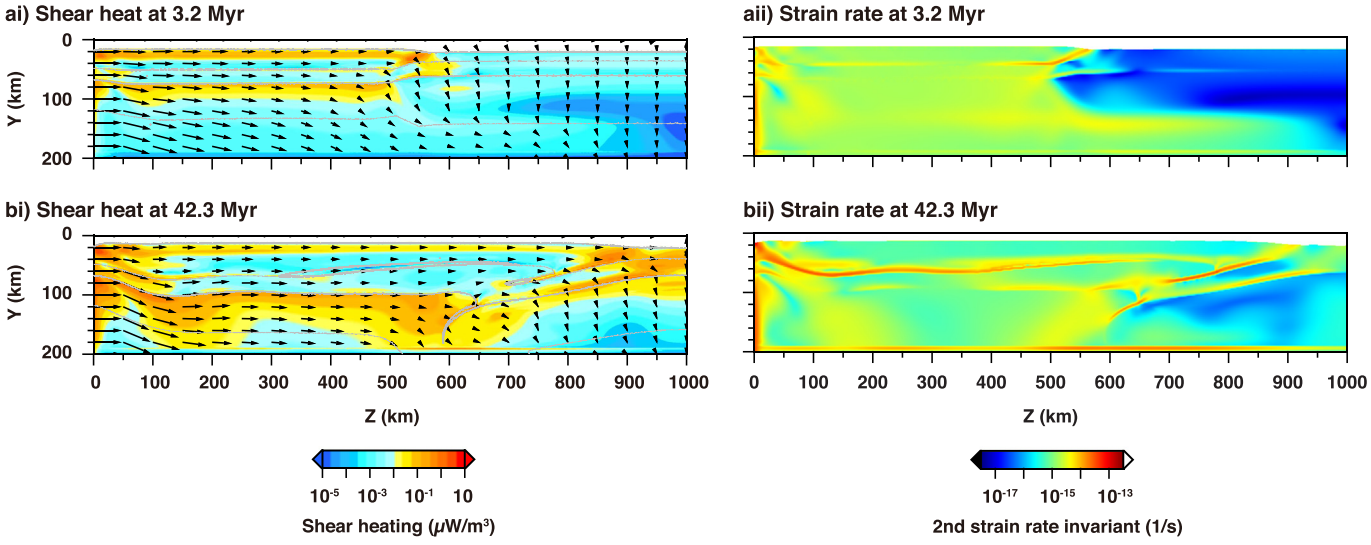

Fig. 10. Evolution of shear heating and strain rate during convergence. **i**, cross-sections of shear heating cutting through the reference model along X = 250 km at **a** 3.2 and **b** 42.3 Myr. **ii**, cross-sections of the second strain rate invariant cutting through the reference model along X = 250 km. The gray lines are material contours, and the black arrows represent the velocity vectors showing the direction of motion.

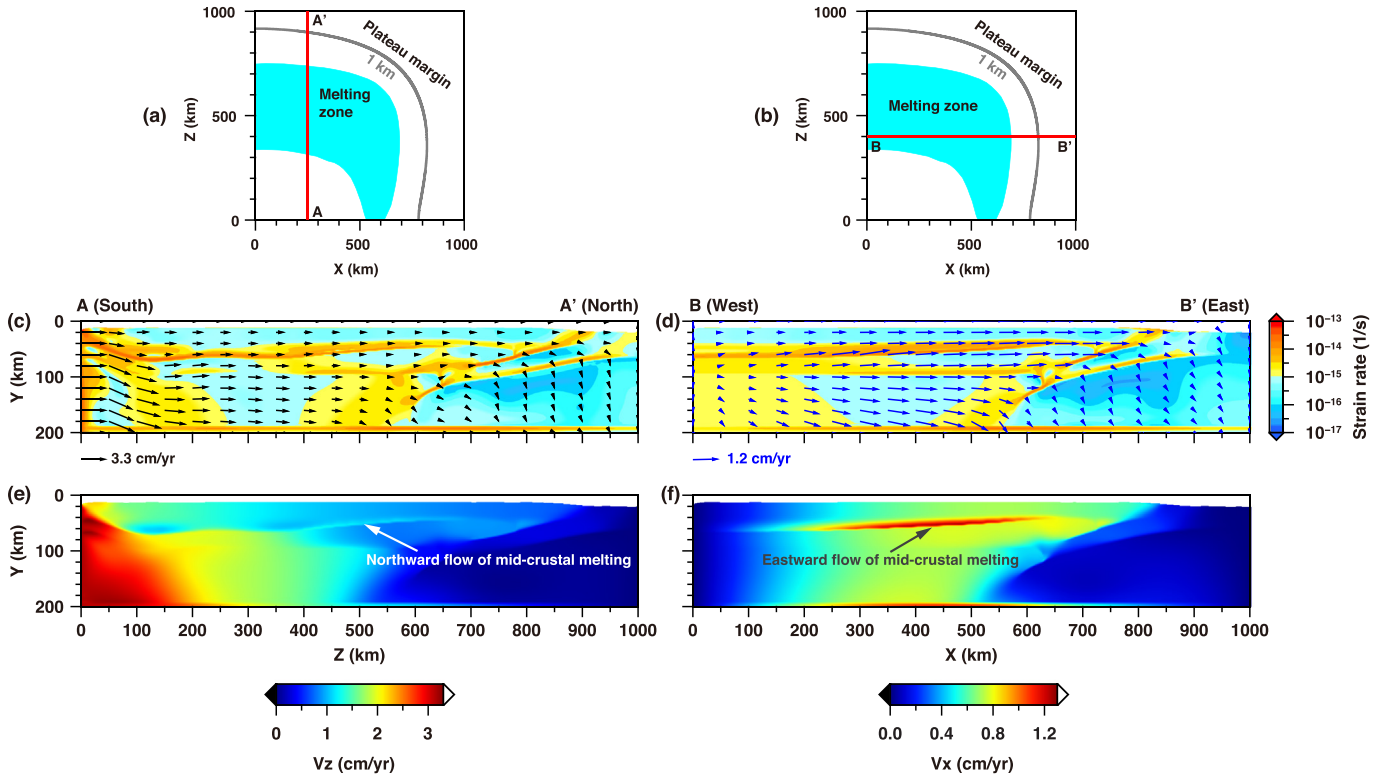

Fig. 11. Typical cross-sections of the second strain rate invariant and velocity vector. The results are for the reference model (Model 1; see Table 2 for details) at 42.3 Myr. The top row shows the plane view of the crustal melting area (i.e., cyan-colored region) and plateau margin (denoted by gray curve) and the localities of the cross-sections (denoted by red lines). The middle row shows the cross-sections of the second strain rate invariant along the lines of X = 250 km (i.e., AA′ in **a**) and of Z = 400 km (i.e., BB′ in **b**), respectively. The velocity fields indicated by the black and blue arrows are superimposed onto the corresponding strain rate sections, which have different scale legends. The bottom row shows the magnitude of the horizontal velocity component along the corresponding cross-section. Specifically, **e** and **f** show the magnitude of V_z and V_x, respectively. (For interpretation of the references to color in this figure legend, the reader is referred to the web version of this article.)

crust because the thermal state of the plateau crust at that time gets much hotter. The thermal and rheological consequences as observed in Model 6 will hold for a later stage-basal heating case.

6. Conclusions

In this study, we investigate the physical controls of mid-crustal melting during collisional orogenesis and explore its consequences on the evolution of orogenic plateaus using 3-D thermo-mechanical models. Our results demonstrate the following:

1) The continued convergence causes orogenic crust to redistribute and in particular to have increasing upper crustal compositions and more radiogenic elements. The resulting radioactive and shear heating provides heat source required for in situ partial melting of deep-buried (at mid-crustal depths) felsic rocks. The amount of mid-crustal partial melting strongly depends on convergence rate. Slower convergence rate favors earlier emergence and larger concentration of mid-crustal melt.
2) Radioactive heating accumulated during crustal thickening plays the primary role in generating mid-crustal partial melting. This is consistent with previous 2-D model results. Shear heating promotes crustal melting, but its role is secondary to radioactive heating. Basal heating may be another important heat source in particular settings (e.g., slab breakoff or lithospheric delamination). Our simulations show that basal heating produces a broad-area increase of the crust temperature and surface elevation and, to a lesser extent, promotes mid-crustal melting, because lateral heat advection driven by convergence dominates the transport of the newly-added heat.
3) The occurrence of mid-crustal partial melting results in a profound reduction of crustal strength. At the later stage of orogenic plateau evolution, the melt-weakened mid-crustal layer flows northward and eastward in a localized channel and leads to differential motion of the layers above and below the melt channel and the marginal dominance of mid-crustal partial melting.
4) We suggest that the widespread low velocity or resistivity zones observed within the Tibetan plateau crust are caused by deep crustal melting. The deep crustal melting is a later-stage product during the tectonic evolution of the Tibetan plateau, not an active control. Mid-crustal melting is pervasive beneath the Tibetan plateau, and the scattered felsic igneous rocks exposed at the extensional rifts or large-scale faults are likely the surficial expression of the widespread mid-crustal melting.

Supplementary data to this article can be found online at https://doi.org/10.1016/j.tecto.2019.03.014.

Acknowledgements

We thank Lijun Liu, Huajian Yao, Christopher Beaumont, William Moore and David Whipp for comments on the early draft. Constructive and thoughtful comments by Weronika Gorczyk, Chris Clark and editor Zheng-Xiang Li substantially improved the manuscript. Open-source software ParaView (http://www.paraview.org) was used for 3-D visualization. This study is supported by the Strategic Priority Research Program (B) of the Chinese Academy of Sciences (XDB18000000), by the National Key Research and Development of China (2016YFC0600406), and by the National Natural Science Foundation of China (41888101, 41474084) to LC. The simulations were run on the TianHe-1A cluster at National Supercomputer Center in Tianjin. The

data for this paper are available by contacting the corresponding author at sinica.lin@gmail.com.

References

Arzi, A.A., 1978. Critical phenomena in the rheology of partially melted rocks. Tectonophysics 44, 173–184.

Bai, D., et al., 2010. Crustal deformation of the eastern Tibetan Plateau revealed by magnetotelluric imaging. Nat. Geosci. 3 (5), 358–362. https://doi.org/10.1038/ngeo830.

Bao, X., Song, X., Li, J., 2015. High-resolution lithospheric structure beneath Mainland China from ambient noise and earthquake surface-wave tomography. Earth Planet. Sci. Lett. 417, 132–141.

Beaumont, C., Jamieson, R.A., Nguyen, M.H., Lee, B., 2001. Himalayan tectonics explained by extrusion of a low-viscosity crustal channel coupled to focused surface denudation. Nature 414, 738–742. https://doi.org/10.1038/414738a.

Beaumont, C., Jamieson, R.A., Nguyen, M.H., Medvedev, S., 2004. Crustal channel flows: 1. Numerical models with applications to the tectonics of the Himalayan-Tibetan orogen. J. Geophys. Res. 109, B06406. https://doi.org/10.1029/2003JB002809.

Bird, P., 1979. Continental delamination and the Colorado Plateau. J. Geophys. Res. 84 (B13), 7561–7571.

Bittner, D., Schmeling, H., 1995. Numerical modeling of melting processes and induced diapirism in the lower crust. Geophys. J. Int. 123, 59–70. https://doi.org/10.1111/J.1365-246x.1995.Tb06661.X.

Brown, M., 2007. Crustal melting and melt extraction, ascent and emplacement in orogens: mechanisms and consequences. J. Geol. Soc. 164, 709–730. https://doi.org/10.1144/0016-76492006-171.

Brown, M., 2010. Melting of the continental crust during orogenesis: the thermal, rheological, and compositional consequences of melt transport from lower to upper continental crust. Can. J. Earth Sci. 47, 655–694. https://doi.org/10.1139/e09-057.

Brune, S., Popov, A.A., Sobolev, S.V., 2012. Modeling suggests that oblique extension facilitates rifting and continental break-up. J. Geophys. Res. 117, B08402. https://doi.org/10.1029/2011JB008860.

Burg, J.P., Gerya, T.V., 2005. The role of viscous heating in Barrovian metamorphism of collisional orogens: thermomechanical models and application to the Lepontine Dome in the Central Alps. J. Metamorph. Geol. 23, 75–95.

Cao, W., Kaus, B.J., Paterson, S., 2016. Intrusion of granitic magma into the continental crust facilitated by magma pulsing and dike-diapir interactions: numerical simulations. Tectonics 35, 1575–1594.

Chen, L., Gerya, T.V., 2016. The role of lateral lithospheric strength heterogeneities in orogenic plateau growth: insights from 3-D thermo-mechanical modeling. J. Geophys. Res. Solid Earth 121, 3118–3138. https://doi.org/10.1002/2016JB012872.

Chung, S.L., et al., 2003. Adakites from continental collision zones: melting of thickened lower crust beneath southern Tibet. Geology 31 (11), 1021–1024. https://doi.org/10.1130/g19796.1.

Chung, S.L., et al., 2005. Tibetan tectonic evolution inferred from spatial and temporal variations in post-collisional magmatism. Earth Sci. Rev. 68 (3–4), 173–196.

Clark, M.K., Royden, L.H., 2000. Topographic ooze: building the eastern margin of Tibet by lower crustal flow. Geology 28 (8), 703–706.

Clark, C., Fitzsimons, I.C.W., Healy, D., Harley, S.L., 2011. How does the continental crust get really hot? Elements 7, 235–240.

Clauser, C., Huenges, E., 1995. Thermal conductivity of rocks and minerals. In: Ahrens, T.J. (Ed.), Rock Physics and Phase Relations, AGU Ref. Shelf. vol. 3. AGU, Washington, D. C, pp. 105–126.

Cook, K.L., Royden, L.H., 2008. The role of crustal strength variations in shaping orogenic plateaus, with application to Tibet. J. Geophys. Res. 113, B08407. https://doi.org/10.1029/2007JB005457.

Cottle, J.M., Larson, K.P., Kellett, D.A., 2015. How does the mid-crust accommodate deformation in large, hot collisional orogens? A review of recent research in the Himalayan orogeny. J. Struct. Geol. 78, 119–133. https://doi.org/10.1016/j.jsg.2015.06.008.

Crameri, F., Schmeling, H., Golabek, G.J., Duretz, T., Orendt, R., Buiter, S.J.H., May, D., Kaus, B.J.P., Gerya, T.V., Tackley, P.J., 2012. A comparison of numerical surface topography calculations in geodynamic modelling: an evaluation of the 'sticky air' method. Geophys. J. Int. 189 (1), 38–54. https://doi.org/10.1111/j.1365-246X.2012.05388.x.

Davies, J.H., von Blanckenburg, F., 1995. Slab breakoff: a model of lithosphere detachment and its test in the magmatism and deformation of collisional orogens. Earth Planet. Sci. Lett. 129, 85–102.

DeCelles, P.G., Robinson, D.M., Zandt, G., 2002. Implications of shortening in the Himalayan fold-thrust belt for uplift of the Tibetan Plateau. Tectonics 21 (6), 1062. https://doi.org/10.1029/2001TC001322.

Ding, L., Kapp, P., Zhong, D.L., Deng, W.M., 2003. Cenozoic volcanism in Tibet: evidence for a transition from oceanic to continental subduction. J. Petrol. 44, 1833–1865.

Ding, L., Xu, Q., Yue, Y., Wang, H., Cai, F., Li, S., 2014. The Andean-type Gangdese Mountains: paleoelevation record from the Paleocene-Eocene Linzhou Basin. Earth Planet. Sci. Lett. 392, 250–264. https://doi.org/10.1016/j.epsl.2014.01.045.

England, P., Houseman, G.A., 1988. The mechanics of the Tibetan Plateau. Philos. Trans. R. Soc. London, Ser. A 326, 301–319.

England, P., Molnar, P., 1993. The interpretation of inverted metamorphic isograds using simple physical calculations. Tectonics 12 (1), 145–157. https://doi.org/10.1029/92TC00850.

Faccenda, M., Gerya, T.V., Chakraborty, S., 2008. Styles of post-subduction collisional orogeny: influence of convergence velocity, crustal rheology and radiogenic heat production. Lithos 103 (1–2), 257–287. https://doi.org/10.1016/j.lithos.2007.09.009.

Furlong, K.P., Chapman, D.S., 2013. Heat flow, heat generation, and the thermal state of the lithosphere. Annu. Rev. Earth Planet. Sci. 41, 385–410. https://doi.org/10.1146/annurev.earth.031208.100051.

Gerya, T.V., 2010. Introduction to Numerical Geodynamic Modelling. 338 pp.. Cambridge Univ. Press, London.

Grujic, D., Casey, M., Davidson, C., Hollister, L.S., Kundig, R., Pavlis, T., Schmid, S., 1996. Ductile extrusion of the Higher Himalayan Crystalline in Bhutan: evidence from quartz microfabrics. Tectonophysics 260, 21–43.

Grujic, D., Hollister, L., Parrish, R., 2002. Himalayan metamorphic sequence as an orogenic channel: insight from Bhutan. Earth Planet. Sci. Lett. 198, 177–191. https://doi.org/10.1016/S0012-821X(02)00482-X.

Guillot, S., Garzanti, E., Baratoux, D., Marquer, D., Mahéo, G., de Sigoyer, J., 2003. Reconstructing the total shortening history of the NW Himalaya. Geochem. Geophys. Geosyst. 4 (7), 1064. https://doi.org/10.1029/2002GC000484.

Hacker, B.R., Gnos, E., Ratschbacher, L., Grove, M., McWilliams, M., Sobolev, S.V., Wan, J., Wu, Z.H., 2000. Hot and dry deep crustal xenoliths from Tibet. Science 287 (5462), 2463–2466. https://doi.org/10.1126/science.287.5462.2463.

Hacker, B.R., Kelemen, P.B., Behn, M.D., 2015. Continental lower crust. Annu. Rev. Earth Planet. Sci. 43, 167–205.

Harris, N., 2007. Channel flow and the Himalayan–Tibetan orogen: a critical review. J. Geol. Soc. 164, 511–523.

Hess, P.C., 1989. Origin of Igneous Rocks. Harvard Univ. Press, London.

Hetenyi, G., Vergne, J., Bollinger, L., Cattin, R., 2011. Discontinuous low-velocity zones in southern Tibet question the viability of the channel flow model. In: Gloaguen, R., Ratschbacher, L. (Eds.), Growth and Collapse of the Tibetan Plateau. Geol. Soc. London Spec. Publ 353. pp. 99–108.

Hirschmann, M.M., 2000. Mantle solidus: Experimental constraints and the effects of peridotite composition. Geochem. Geophys. Geosyst. https://doi.org/10.1029/2000GC000070.

Houseman, G., Molnar, P., 2001. Mechanisms of lithospheric rejuvenation associated with continental orogeny. In: Miller, J.A., Holdsworth, R.E., Buick, I.S., Hand, M. (Eds.), Continental Reactivation and Reworking. Geol. Soc. London Spec. Publ 184. pp. 13–38.

Jamieson, R.A., Beaumont, C., 2013. On the origin of orogens. GSA Bull. 125, 1671–1702.

Jamieson, R.A., Beaumont, C., Fullsack, P., Lee, B., 1998. Barrovian regional metamorphism: where's the heat? In: Treloar, P.J., O'Brien, P.J. (Eds.), What Drives Metamorphism and Metamorphic Reactions? Geol. Soc. London Spec. Publ 138. pp. 23–51.

Jamieson, R.A., Unsworth, M.J., Harris, N.B.W., Rosenberg, C.L., Schulmann, K., 2011. Crustal melting and the flow of mountains. Elements 7 (4), 253–260. https://doi.org/10.2113/gselements.7.4.253.

Jimenez-Munt, I., Platt, J.P., 2006. Influence of mantle dynamics on the topographic evolution of the Tibetan Plateau: results from numerical modeling. Tectonics 25, TC6002. https://doi.org/10.1029/2006TC001963.

Johannes, W., 1985. The significance of experimental studies for the formation of migmatites. In: Ashworth, J.R. (Ed.), Migmatites. Blackie, Glasgow, U. K., pp. 36–85.

Kapp, P., Yin, A., Harrison, T.M., Ding, L., 2005. Cretaceous-tertiary shortening, basin development, and volcanism in central Tibet. Geol. Soc. Am. Bull. 117 (7–8), 865–878. https://doi.org/10.1130/b25595.1.

Katz, R.F., Spiegelman, M., Langmuir, C.H., 2003. A new parameterization of hydrous mantle melting. Geochem. Geophys. Geosyst. 4 (9), 1073. https://doi.org/10.1029/2002GC000433.

Katz, R.F., Spiegelman, M., Holtzman, B., 2006. The dynamics of melt and shear localization in partially molten aggregates. Nature 442, 676–679. https://doi.org/10.1038/nature05039.

Kay, R.W., Kay, S.M., 1993. Delamination and delamination magmatism. Tectonophysics 219, 177–189.

Keller, T., May, D.A., Kaus, B.J., 2013. Numerical modelling of magma dynamics coupled to tectonic deformation of lithosphere and crust. Geophys. J. Int. 195, 1406–1442.

Klemperer, S.L., 2006. Crustal flow in Tibet: geophysical evidence for the physical state of Tibetan lithosphere, and inferred patterns of active flow. In: Law, R.D., Searle, M.P., Godin, L. (Eds.), Channel Flow, Ductile Extrusion and Exhumation in Continental Collision Zones. Geol. Soc. London Spec. Publ 268. pp. 39–70.

McKenzie, D., Priestley, K., 2008. The influence of lithospheric thickness variations on continental evolution. Lithos 102, 1–11.

Medvedev, S., Beaumont, C., 2006. Growth of continental plateaus by channel injection: models designed to address constraints and thermomechanical consistency. In: Law, R.D., Searle, M.P., Godin, L. (Eds.), Channel Flow, Ductile Extrusion and Exhumation in Continental Collision Zones. Geological Society, London, Special Publications 268. pp. 147–164. https://doi.org/10.1144/gsl.sp.2006.268.01.06.

Molnar, P., England, P., Martinod, J., 1993. Mantle dynamics, uplift of the Tibetan plateau, and the Indian Monsoon. Rev. Geophys. 31 (4), 357–396. https://doi.org/10.1029/93RG02030.

Murphy, M.A., Yin, A., Harrison, T.M., Durr, S.B., Chen, Z., Ryerson, F.J., Kidd, W.S.F., Wang, X., Zhou, X., 1997. Did the Indo-Asian collision alone create the Tibetan Plateau? Geology 25 (8), 719–722.

Nabelek, P.I., Whittington, A.G., Hofmeister, A.M., 2010. Strain heating as a mechanism for partial melting and ultrahigh temperature metamorphism in convergent orogens: implications of temperature-dependent thermal diffusivity and rheology. J. Geophys. Res. 115, B12417. https://doi.org/10.1029/2010JB007727.

Nelson, K.D., et al., 1996. Partially molten middle crust beneath southern Tibet: synthesis of project INDEPTH results. Science 274 (5293), 1684–1688. https://doi.org/10.1126/science.274.5293.1684.

Owens, T.J., Zandt, G., 1997. Implications of crustal property variations for models of

Tibetan Plateau evolution. Nature 387 (6628), 37–43. https://doi.org/10.1038/387037a0.
Poli, S., Schmidt, M.W., 2002. Petrology of subducted slabs. Annu. Rev. Earth Planet. Sci. 30, 207–235. https://doi.org/10.1146/annurev.earth.30.091201.140550.
Ranalli, G., 1995. Rheology of the Earth: Deformation and Flow Processes in Geophysics and Geodynamics, 2nd ed. Chapman and Hall, London.
Rey, P., Teyssier, C., Whitney, D.L., 2010. Limit of channel flow in orogenic plateau. Lithosphere 2 (5), 328–332. https://doi.org/10.1130/l114.1.
Rosenberg, C.L., Handy, M.R., 2005. Experimental deformation of partially melted granite revisited: implications for the continental crust. J. Metamorph. Geol. 23, 19–28.
Rosenberg, C.L., Medvedev, S., Handy, M., 2007. On the effects of melting on continental deformation and faulting. In: Handy, M., Hirth, G., Hovius, N. (Eds.), Tectonic Faults: Agents of Change on a Dynamic Earth. Dahlem Workshop Report 95 MIT Press, pp. 357–402.
Royden, L.H., Burchfiel, B.C., King, R.W., Wang, E., Chen, Z.L., Shen, F., Liu, Y.P., 1997. Surface deformation and lower crustal flow in eastern Tibet. Science 276 (5313), 788–790. https://doi.org/10.1126/science.276.5313.788.
Royden, L.H., Burchfiel, B.C., van der Hilst, R.D., 2008. The geological evolution of the Tibetan plateau. Science 321, 1054–1058.
Rudnick, R.L., Fountain, D.M., 1995. Nature and composition of the continental crust: a lower crustal perspective. Rev. Geophys. 33, 267–309.
Rudnick, R.L., Gao, S., 2014. Composition of the Continental Crust. 2014. See Holland & Turekian, pp. 1–51.
Schmidt, M.W., Poli, S., 1998. Experimentally based water budgets for dehydrating slabs and consequences for arc magma generation. Earth Planet. Sci. Lett. 163, 361–379. https://doi.org/10.1016/S0012-821X(98)00142-3.
Shapiro, N.M., Ritzwoller, M.H., Molnar, P., Levin, V., 2004. Thinning and flow of Tibetan crust constrained by seismic anisotropy. Science 305, 233–236. https://doi.org/10.1126/science.1098276.
Shen, F., Royden, L.H., Burchfiel, B.C., 2001. Large-scale crustal deformation of the Tibetan Plateau. J. Geophys. Res. 106, 6793–6816. https://doi.org/10.1029/2000JB900389.
Styron, R.H., Taylor, M.H., Murphy, M.A., 2011. Oblique convergence, arc-parallel extension, and the role of strike-slip faulting in the High Himalaya. Geosphere 7, 1–15.
Turcotte, D.L., Schubert, G., 2002. Geodynamics. Cambridge Univ. Press, Cambridge, U. K.
Unsworth, M.J., Jones, A.G., Wei, W., Marquis, G., Gokarn, S.G., Spratt, J.E., Team, I.-M., 2005. Crustal rheology of the Himalaya and Southern Tibet inferred from magnetotelluric data. Nature 438 (7064), 78–81. https://doi.org/10.1038/nature04154.
Vanderhaeghe, O., Teyssier, C., 2001. Partial melting and flow of orogens. Tectonophysics 342 (3–4), 451–472.
Vergne, J., Wittlinger, G., Hui, Q., Tapponnier, P., Poupinet, G., Mei, J., Herquel, G., Paul, A., 2002. Seismic evidence for stepwise thickening of the crust across the NE Tibetan plateau. Earth Planet. Sci. Lett. 203, 25–33.
Wang, Q., et al., 2010. Eocene north-south trending dikes in central Tibet: New constraints on the timing of east-west extension with implications for early plateau uplift. Earth Planet. Sci. Lett. 298, 205–216.
Wang, Q., et al., 2012. Crustal melting and flow beneath Northern Tibet: evidence from Mid-Miocene to Quaternary strongly peraluminous rhyolites in the Southern Kunlun range. J. Petrol. 53 (12), 2523–2566. https://doi.org/10.1093/petrology/egs058.
Wei, W.B., et al., 2001. Detection of widespread fluids in the Tibetan crust by magnetotelluric studies. Science 292 (5517), 716–718. https://doi.org/10.1126/science.1010580.
Whipple, K.X., 2009. The influence of climate on the tectonic evolution of mountain belts. Nat. Geosci. 2 (2), 97–104. https://doi.org/10.1038/ngeo413.
Whitney, D.L., Teyssier, C., Rey, P.F., 2009. The consequences of crustal melting in continental subduction. Lithosphere 1 (6), 323–327. https://doi.org/10.1130/l62.1.
Yang, Y., Ritzwoller, M.H., Zheng, Y., Shen, W., Levshin, A.L., Xie, Z., 2012. A synoptic view of the distribution and connectivity of the mid-crustal low velocity zone beneath Tibet. J. Geophys. Res. 117, B04303. https://doi.org/10.1029/2011JB008810.
Yin, A., Harrison, T.M., 2000. Geologic evolution of the Himalayan-Tibetan orogen. Annu. Rev. Earth Planet. Sci. 28, 211–280.
Zhao, L.-F., Xie, X.-B., He, J.-K., Tian, X., Yao, Z.-X., 2013. Crustal flow pattern beneath the Tibetan Plateau constrained by regional Lg-wave Q tomography. Earth Planet. Sci. Lett. 383, 113–122. https://doi.org/10.1016/j.epsl.2013.09.038.